

MMedExpert-R1: Strengthening Multimodal Medical Reasoning via Domain-Specific Adaptation and Clinical Guideline Reinforcement

Meidan Ding^{1,2,3,†}, Jipeng Zhang^{4,†}, Wenvxuan Wang⁵, Haiqin Zhong⁶,
Xiaoling Luo¹ Wenting Chen⁷, Linlin Shen^{1,2,3}

¹College of Computer Science and Software Engineering, Shenzhen University

²School of Artificial Intelligence, Shenzhen University ⁷Stanford University

³Guangdong Provincial Key Laboratory of Intelligent Information Processing

⁴The Hong Kong University of Science and Technology ⁵Renmin University of China

⁶School of Biomedical Engineering, Shenzhen University

Abstract

Medical Vision-Language Models (MedVLMs) excel at perception tasks but struggle with complex clinical reasoning required in real-world scenarios. While reinforcement learning (RL) has been explored to enhance reasoning capabilities, existing approaches face critical mismatches: the scarcity of deep reasoning data, cold-start limits multi-specialty alignment, and standard RL algorithms fail to model clinical reasoning diversity. We propose MMedExpert-R1, a novel reasoning MedVLM that addresses these challenges through domain-specific adaptation and clinical guideline reinforcement. We construct MMedExpert, a high-quality dataset of 10K samples across four specialties with step-by-step reasoning traces. Our Domain-Specific Adaptation (DSA) creates specialty-specific LoRA modules to provide diverse initialization, while Guideline-Based Advantages (GBA) explicitly models different clinical reasoning perspectives to align with real-world diagnostic strategies. Conflict-Aware Capability Integration then merges these specialized experts into a unified agent, ensuring robust multi-specialty alignment. Comprehensive experiments demonstrate state-of-the-art performance, with our 7B model achieving 27.50 on MedXpert-MM and 83.03 on OmniMedVQA, establishing a robust foundation for reliable multimodal medical reasoning systems.

1 Introduction

Medical Vision-Language Models (MedVLMs) have proven effective in medical analysis (Acosta et al., 2022) and assistive diagnosis (Lipkova et al., 2022), achieving promising results in tasks such as medical report generation (Che et al., 2025) and disease classification (Jin et al., 2024). However, deploying these models in complex clinical scenarios often yields suboptimal performance. This stems from a critical capability gap: while existing MedVLMs are predominantly perception-

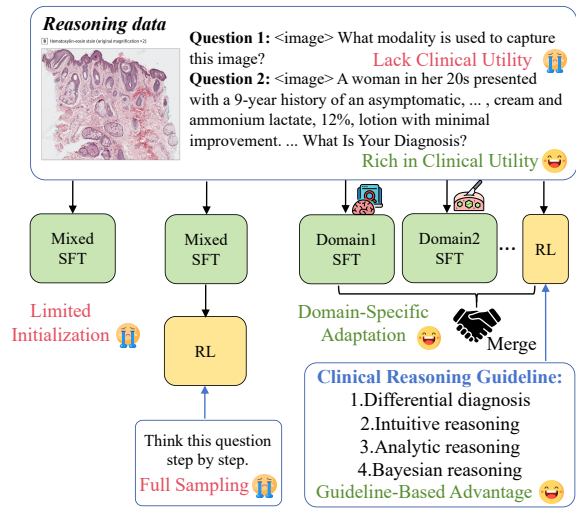


Figure 1: The core elements in MMedExpert-R1. The framework combines **Domain-Specific Adaptation (DSA)** through specialty-aware LoRA modules, **Clinical Reasoning Data** from mixed medical cases across multiple domains, and **Guideline-Based Advantage** estimation guided by clinical reasoning guidelines.

oriented, they lack the sophisticated reasoning capabilities required to handle real-world clinical contexts. Specifically, clinical decision-making necessitates reasoning over diverse and interdependent information sources, synthesizing longitudinal patient data, and incorporating contextual medical knowledge, which remains a challenge for current perception-based approaches (Su et al., 2025).

To overcome this limitation, reinforcement learning (RL) methods have been explored to bridge the gap between perception and reasoning, following their proven success in general scenarios like math (Liu et al., 2025) and code generation (Yang et al., 2025). A prominent stream involves leveraging RL algorithms, such as GRPO (Guo et al., 2025), during post-training to foster Chain of Thought (CoT) reasoning and self-reflection (e.g., Med-R1 (Lai et al., 2025) and MedVLM-R1 (Pan et al., 2025)). These methods optimize the model

by maximizing rule-based rewards, thereby explicitly encouraging robust clinical reasoning.

Though satisfactory performance, there are still **some mismatches** in reasoning MedVLMs with the elements of RL (Lai et al., 2025; Pan et al., 2025; Su et al., 2025), as shown in Figure 1.

Firstly, the difficulty of training data does not match clinical needs. Current multimodal medical datasets (Chen et al., 2024; Zhang et al., 2023) predominantly involve visual perception and shallow understanding tasks, whereas clinical questions demand step-wise differential diagnosis and evidence synthesis. In the elements of RL, the lack of deep reasoning supervision not only undermines data effectiveness but also prevents the reward signals from faithfully reflecting the true value of clinical reasoning. These observations motivate us to collect high-quality clinical data, which includes images, clinical records, and patient histories.

Secondly, the RL with cold start limits multi-specialty alignment. The standard RL pipeline is typically initialized from a single Supervised Fine-Tuning (SFT) checkpoint, effectively functioning as behavior cloning (Su et al., 2025; Huang et al., 2025). This paradigm yields a low-entropy policy that rigidly mimics the narrow distribution of the training data. In medicine, where clinical scenarios span diverse sub-specialties, this limitation is particularly severe: training data should cover varied specialties, yet the constrained initialization creates a "cold start" problem that restricts generation of diverse reasoning candidates. Thus, it is necessary to diversify the model distribution to expand the policy's exploration horizon and ensure robust alignment across distinct clinical paradigms.

Thirdly, naive adoption of RL algorithms (e.g., GRPO) lacks medical domain modeling. Although GRPO achieves stable optimization in general reasoning tasks, it shows clear limitations in medical scenarios. Its full-sampling assumption treats all reasoning trajectories as independent and equivalent, ignoring the diverse and complementary perspectives involved in real-world clinical decision-making. This clinical reasoning diversity—a core feature of medical cognition—should be explicitly modeled in RL sampling. In the elements of RL, the advantage function fails to differentiate reasoning quality, leading the model to overfit a single thinking pattern. Thus, it is essential to incorporate diverse reasoning paths into the RL process to align the model with real-world expert logic.

Overall, the mismatch across RL elements results in unstable optimization and poor generalization to real-world clinical reasoning. Addressing these systemic limitations is critical for developing reliable and clinically grounded multimodal reasoning models.

To overcome the aforementioned mismatches, we propose **MMedExpert-R1**, a novel reasoning MedVLM designed to cultivate reliable clinical reasoning by systematically enhancing the core elements of Reinforcement Learning, as illustrated in Figure 1. To bridge the data complexity gap, we **construct a high-quality medical reasoning dataset MMedExpert** with 3.9K samples from four key specialties. Unlike standard VQA pairs, each entry couples a clinical scenario with a rigorous, step-by-step reasoning trace, providing the dense supervision required to model expert cognition. Based on this dataset, to provide multi-specialty model initialization, we propose a **Domain-Specific Adaptation (DSA) paradigm** to circumvent the exploration bottleneck inherent in standard checkpoints. DSA builds upon domain-aware LoRA modules, each fine-tuned on a single-specialty data, yielding expert models for each specialty. These modules recalibrate the initial policy distribution to cover a wider semantic manifold, preventing the agent from collapsing into suboptimal modes and providing a navigable search space for subsequent RL optimization. Meanwhile, to align optimization with the nuance of real-world clinical decision-making, we introduce a **Guideline-Based Advantages (GBA)** module. This mechanism explicitly models diverse reasoning perspectives (e.g., differential vs. intuitive) with the advantages based on different clinical guidelines, enabling the policy to differentiate between high-quality diagnostic strategies and formulaic text generation rigorously. For the multi-specialty alignment issue of RL with cold start, we propose a **Conflict-Aware Capability Integration** to finally merge the experts models from DSA and GBA into a unified reasoning agent to synthesize the dispersed capabilities. MMedExpert-R1 enhances core RL components—training data quality, checkpoint design, and the advantage function—enabling more effective RL in medical contexts and producing clearer, clinically grounded reasoning. Extensive experiments demonstrate the superiority of MMedExpert-R1 to current LLMs across four datasets. Overall, our contributions are as follows:

- We introduce MMedExpert, a high-quality, clinical reasoning dataset enriched with structured, step-by-step reasoning traces to support deeper and more interpretable clinical cognition.
- We propose MMedExpert-R1, a novel reasoning MedVLM that cultivates specialized and reliable clinical reasoning by refining key elements of reinforcement learning.
- We propose Domain-Specific Adaptation (DSA) and Guideline-Based Advantages (GBA) to improve RL-based medical reasoning, addressing limited generalization through domain-grounded initialization and enhancing reasoning diversity via guideline-based advantages.
- Extensive experiments demonstrate the superiority of our MMedExpert-R1 to four existing medical benchmarks.

2 Related Work

2.1 Medical Vision-Language Model

The rapid development of Vision-Language Model (VLM) has led to remarkable advances across diverse domains, generating substantial interest in their application to the medical field (Tian et al., 2023; AlSaad et al., 2024). Early studies sought to integrate LLMs with specialized medical vision encoders, typically through a linear transformation layer, in order to achieve vision–language alignment for medical image understanding and analysis (Li et al., 2023; Moor et al., 2023; Liu et al., 2023; Zhang et al., 2024a). Building upon this foundation, subsequent research has largely retained similar architectural paradigms while introducing a variety of strategies to improve performance. These strategies include constructing more comprehensive training datasets (Ikezogwo et al., 2023; Chen et al., 2024; Li et al., 2024; Hamamci et al., 2024), designing sophisticated training recipes (Nath et al., 2025; Wang et al., 2024), employing efficient fine-tuning techniques (Lin et al., 2025), incorporating mixture-of-experts mechanisms (He et al., 2024), and leveraging reinforcement learning (Lai et al., 2025; Pan et al., 2025). Building upon these developments, our work presents MMedExpert-R1, which incorporates domain-grounded initialization and clinical guideline reinforcement, enhancing both diagnostic reasoning and medical reliability.

2.2 RL in MedVLMs

Recent studies have applied reinforcement learning (RL) to enhance medical reasoning, leading to significant gains in accuracy, interpretability, and generalization. Models such as Med-R1 (Lai et al., 2025) and MedVLM-R1 (Pan et al., 2025) leverage GRPO to refine reasoning trajectories rather than relying solely on supervised fine-tuning, enabling more reliable decision-making across complex medical imaging tasks. Similarly, GMAI-VL-R1 (Su et al., 2025) integrates RL-based tuning with multi-modal data fusion, strengthening chain-of-thought reasoning and clinical robustness. Despite this progress, current MedVLMs still exhibit inconsistencies between their medical reasoning processes and the core elements of reinforcement learning. These structural mismatches hinder the full potential of RL in medical domains. Therefore, we aim to cultivate specialized, robust, and trustworthy clinical reasoning by systematically refining the key components of the RL framework for MedVLMs.

2.3 Model Merging

Model merging integrates complementary capabilities from multiple source models, yielding a single unified network directly within the parameter space. As a parameter-efficient optimization problem, merging algorithms calibrate the weight coefficients or resolve parameter interference to encode diverse functional skills, considering both task-specific knowledge and general representations. Recently, model merging has been extended to cross-modal integration and heterogeneous architecture fusion to model complex reasoning capabilities. (Yang et al., 2024). Chen et al. (2025) proposes merging models across modalities, effectively enabling the incorporation of the superior reasoning capabilities of LLMs into VLMs. Zhang et al. (2024b) further proposes an unconstrained framework that accommodates both homogeneous and heterogeneous architectures. Distinct from the aforementioned heterogeneous model fusion and only-SFT checkpoints fusion, we define the integration of models derived from knowledge-based SFT models and logic-based model RL as a unified merging task. This approach effectively harmonizes domain-specific medical knowledge with rigorous reasoning alignment, bridging the gap between raw professional expertise and preference-driven clinical decision-making.

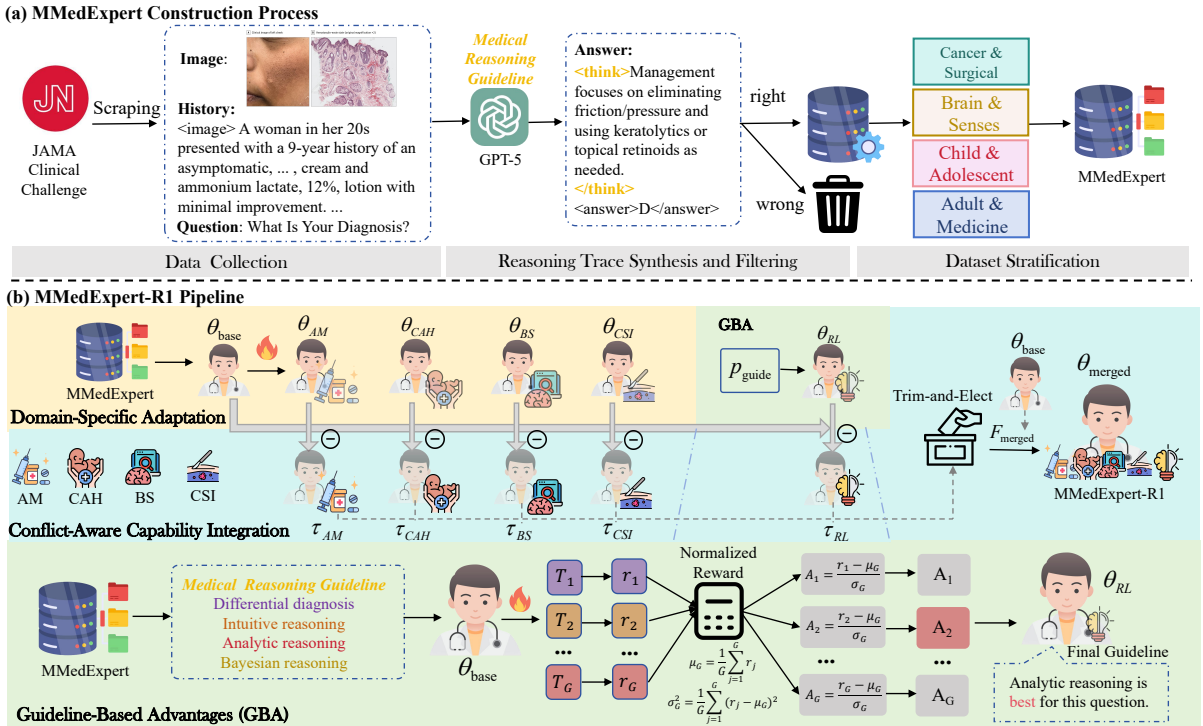


Figure 2: (a) Data construction of **MMedExpert**; (b) **MMedExpert-R1** consists of a Domain-Specific Adaptation to provide diverse initialization, Guideline-Based Advantages to align with real-world diagnostic strategies, and a Conflict-Aware Capability Integration to ensure multi-specialty alignment.

3 MMedExpert

Existing medical Visual Question Answering (VQA) datasets frequently suffer from a complexity gap, lacking the depth required to mirror decision-making processes in real-world clinical settings. To bridge this gap, we introduce *MMedExpert*, a dataset explicitly synthesized to foster high-quality multimodal medical reasoning. Our construction pipeline proceeds in three rigorous stages.

3.1 Data Collection

To establish a robust foundation, we curated a source corpus of 10K raw samples (comprising 8K text-only and 2K multimodal instances) from authoritative clinical databases, including MedUSLM and the JAMA Clinical Challenge. Crucially, the patient histories in this collection average approximately 200 tokens, preserving the narrative intricacy and diagnostic ambiguity inherent in Electronic Health Records (EHRs).

3.2 Reasoning Trace Synthesis and Filtering

To distill expert-level cognitive capabilities, we employed a guideline-driven generation strategy utilizing GPT-5. Departing from generic generation methods, we incorporated structured medical

reasoning guidelines (Savage et al., 2024) as hard constraints. Specifically, the model was instructed to synthesize reasoning traces aligned with four distinct clinical paradigms: (1) *Differential Diagnosis*, (2) *Intuitive Reasoning*, (3) *Analytical Reasoning*, and (4) *Bayesian Reasoning*. (Detailed definitions are provided in Appendix A.) This ensures that the generated chains of thought reflect the diverse cognitive strategies employed by human experts, rather than formulaic textbook patterns.

To ensure data quality, we implemented a rigorous two-stage curation protocol. The first stage automatically filtered sequences based on exact-match accuracy, while the second stage involved manual verification by medical professionals to validate strict adherence to the designated reasoning paradigms. This process yielded a high-quality dataset \mathcal{D} comprising 3.9K samples, stratified into 3.3K text-only and 0.6K multimodal entries.

3.3 Dataset Stratification

Finally, we decompose the dataset \mathcal{D} into four mutually exclusive subsets corresponding to distinct clinical specialties: Adult Medicine (AM), Child and Adolescent Health (CAH), Brain and Senses (BS), and Cancer and Surgical Interven-

tions (*CSI*). This partition is formalized as:

$$\mathcal{D} = \bigcup_{k \in \mathcal{K}} \mathcal{D}_k, \quad (1)$$

where $\mathcal{K} = \{AM, CAH, BS, CSI\}$. Note that these subsets are mutually exclusive, satisfying $\mathcal{D}_i \cap \mathcal{D}_j = \emptyset$ for any $i \neq j$.

4 MMedExpert-R1

Current medical alignment paradigms typically rely on a two-stage framework, where a unified model undergoes Supervised Fine-Tuning (SFT) on pooled data, followed by Reinforcement Learning (RL). While superior to direct RL, which often hallucinates due to a lack of foundational knowledge, this "Single SFT+RL" approach suffers from severe parameter interference. Thus, we propose MMedExpert-R1, a novel decoupled multi-expert framework. Unlike prior methods that force a single parameter set to master all objectives simultaneously, we theoretically disentangle factual acquisition (via Domain-Specific Adaptation) from logical alignment (via Guideline-Based Advantages). By subsequently synthesizing these orthogonal capabilities through a Conflict-Aware Capability Integration, our approach effectively resolves the tension between broad medical knowledge and rigorous reasoning depth.

4.1 Domain-Specific Adaptation (DSA)

To provide diverse clinical model initializations, we introduce a domain-specific adaptation. To efficiently inject specialized knowledge without the prohibitive cost of full-parameter tuning, we employ Low-Rank Adaptation (LoRA). Let θ_{base} denote the frozen backbone parameters. For each sub-domain $k \in \{AM, CAH, BS, CSI\}$, we initialize a specific adapter $\Delta\theta_k$ and optimize it by minimizing the domain-specific SFT loss:

$$\Delta\theta_k^* = \underset{\Delta\theta_k}{\operatorname{argmin}} \mathcal{L}_{\text{SFT}}(\mathcal{D}_k; \theta_{\text{base}} + \Delta\theta_k). \quad (2)$$

This parallel training process yields a set of specialized parameter states, formally defined as:

$$\theta_k = \theta_{\text{base}} + \Delta\theta_k^*. \quad (3)$$

These expert models θ_k encapsulate the distinct semantic distributions of their respective fields, providing the necessary factual basis for the subsequent integration stage.

4.2 Guideline-Based Advantages (GBA)

Since the RL + SFT pipeline limits multi-specialty alignment due to its cold-start nature, we introduce Guideline-Based Advantage (GBA) to align optimization with the nuance of real-world clinical decision-making. Unlike standard reinforcement learning that pursues absolute rewards, GBA leverages group-relative statistics to identify and reinforce reasoning paths that best adhere to medical protocols.

For each medical query Q , we construct a prompt $p \in \mathcal{P}_{\text{guide}}$ containing clinical guidelines. Conditioned on p , we sample a group of G reasoning trajectories $\{y_1, \dots, y_G\}$ from the policy π_θ . Instead of using absolute scores, we compute the relative advantage $\hat{\mathcal{A}}_i$ for each trajectory y_i by normalizing its reward against the group statistics:

$$\begin{aligned} \hat{\mathcal{A}}_i &= \frac{r(p, y_i) - \mu_G}{\sigma_G + \epsilon}, \\ \text{where } \mu_G &= \frac{1}{G} \sum_{i=1}^G r(p, y_i). \end{aligned} \quad (4)$$

Here, $r(p, y_i)$ integrates diagnostic accuracy and structural constraints. Crucially, this normalization isolates the reasoning quality from the query's inherent difficulty. A positive advantage $\hat{\mathcal{A}}_i > 0$ signals superior guideline adherence relative to the group average μ_G , effectively filtering out variance. Finally, we optimize the policy to maximize the likelihood of these high-advantage trajectories. The objective function uses $\hat{\mathcal{A}}_i$ to re-weight the gradient updates:

$$\begin{aligned} \mathcal{J}_{\text{GBA}}(\theta) &= \mathbb{E}_{\substack{p \sim \mathcal{D}, \\ \{y_i\} \sim \pi_\theta}} \left[\frac{1}{G} \sum_{i=1}^G \frac{\hat{\mathcal{A}}_i}{|y_i|} \right. \\ &\quad \left. \cdot \sum_{t=1}^{|y_i|} \log \pi_\theta(y_{i,t} \mid p, y_{i,<t}) \right]. \end{aligned} \quad (5)$$

By explicitly penalizing deviations (where $\hat{\mathcal{A}}_i < 0$) and reinforcing valid chains, this objective shifts the policy distribution towards the guideline-compliant region.

4.3 Conflict-Aware Capability Integration

Since the RL with cold start limits multi-specialty alignment, we introduce Conflict-Aware Capability Integration to fuse various model experts to improve the alignment. Specifically, we obtain two distinct categories of parameter updates: the

knowledge-centric experts $\theta_{\text{AM}}, \theta_{\text{CAH}}, \theta_{\text{BS}}, \theta_{\text{CSI}}$ (encoding factual breadth) and the reasoning-centric model θ_{RL} (encoding logical depth). Naive averaging of these heterogeneous task vectors often precipitates catastrophic interference, where gradient drift from RL optimization overwrites the fine-grained domain features learned during SFT. To address this, we propose a Conflict-Aware Capability Integration strategy utilizing TIES-Merging. We specifically adapt this technique to bridge the gap between distinct optimization objectives, resolving the parameter interference between factual memorization (SFT) and logical alignment (RL).

First, we isolate the capability-specific updates by transforming all fine-tuned models into a unified task vector space:

$$\tau_k = \theta_k - \theta_{\text{base}}, \quad (6)$$

$k \in \{\text{AM, CAH, BS, CSI, RL}\}$. This separates the specific factual and reasoning injections from the base weights. Subsequently, we synthesize a robust specialist using the Trim-and-Elect mechanism:

$$\tau_{\text{merged}} = \mathcal{F}_{\text{TIES}}(\{\tau_k\}; \lambda). \quad (7)$$

The operator $\mathcal{F}_{\text{TIES}}$ filters stochastic noise by retaining only the top- $k\%$ magnitude parameters and enforcing sign consistency. This ensures that only consensual features—validated across multiple domains or reinforced by reasoning alignment—are preserved. The final dual-stream agent is reconstructed via $\theta_{\text{merged}} = \theta_{\text{base}} + \eta \cdot \tau_{\text{merged}}$, effectively harmonizing granular domain knowledge with rigorous clinical logic.

5 Experiments

5.1 Experiment Setting

To comprehensively evaluate the performance of MMedExpert-R1 across a broad range of clinical reasoning tasks, we benchmark it against a diverse set of state-of-the-art medical vision-language models, including MedVLM-R1 (Pan et al., 2025), Med-R1 (Lai et al., 2025), MedVLThinker (Huang et al., 2025), MedGemma (Sellergren et al., 2025), LLaVA-Med (Li et al., 2023), HuatuoGPT-V (Chen et al., 2024), BiMediX2 (Mullappilly et al., 2024), and Lingshu (Xu et al., 2025). To ensure fair and consistent comparisons, all models are assessed within a standardized environment using our proposed MedEvalKit. This framework unifies experimental settings, prompts, and evaluation metrics across all candidate models.

For benchmark datasets, we utilize the test sets of **PMC-VQA (v2)** (Zhang et al., 2023), **Omn-iMedVQA** (Hu et al., 2024), **GMAI-MMBench (val)** (Ye et al., 2024), and **MedXpertQA-MM** (Zuo et al., 2025). Collectively, these benchmarks cover a comprehensive spectrum of medical imaging modalities, spanning X-ray, CT, MRI, PET, ultrasound, microscopy, pathology, OCT, dermatoscopy, gastrointestinal (GI) examinations, endoscopy, and fundus imaging, as well as medical charts, tables, and figures. This extensive coverage ensures a rigorous and holistic assessment of multimodal medical reasoning capabilities. Implementation Details are shown in the Appendix B.

5.2 Experimental Results

We evaluate MMedExpert-R1 against MedVLMs across varying parameter scales (2B and 7B).

5.2.1 Main Results and Scaling Analysis

As presented in Table 1, MMedExpert-R1 demonstrates superior overall performance compared to state-of-the-art MedVLMs across both the 2B and 7B parameter scales. In the lightweight group (< 4B parameters), MMedExpert-R1 (2B) establishes a distinct advantage across multiple benchmarks. It achieves a Total score of 23.35 on MedXpert-MM, surpassing the 3B-scale MedVLThinker (21.90). This superiority extends to external benchmarks, where our 2B model records 53.27 on PMC-VQA and 43.67 on GMAI-MM, significantly outperforming MedVLM-R1 (47.83 and 41.18). Upon scaling to 7B parameters, MMedExpert-R1 achieves comprehensive state-of-the-art results. It secures a leading score of 27.50 on MedXpert-MM, while also dominating public benchmarks with scores of 56.78 on PMC-VQA, 83.03 on OMVQA, and 52.10 on GMAI-MM, consistently exceeding strong competitors like Lingshu (54.68, 82.85, and 51.21) and HuatuoGPT-V.

5.2.2 Fine-grained Analysis of Clinical Capabilities

To further investigate the source of these performance gains, we analyze the model’s proficiency in specific clinical tasks using metrics from both MedXpert-MM (Table 1) and the GMAI-MM validation set (Table 2).

Results from MedXpert-MM highlight MMedExpert-R1’s exceptional capability in high-stakes clinical decision-making. Specifically, our 2B model achieves a "Treatment" score of 28.12,

Table 1: Performance comparison of MMedExpert-R1 with other MedVLMs on medical multimodal benchmarks, where bold indicates the best. Note that OMVQA indicates OmniMedVQA. MedVLM-R1 and Med-R1 is trained on part of the OmniMedVQA test set, making its results on OmniMedVQA meaningless.

Base	Size	MedXpert-MM						PMC-VQA	OMVQA	GMAI-MM
		Total	Rea.	Under.	Treatment	Basic Science	Diagnosis			
MedVLM-R1	2B	19.95	19.84	20.21	20.98	17.28	20.35	47.83	-	41.18
Med-R1	2B	21.15	20.88	21.84	24.33	17.28	21.10	45.48	-	40.79
MedVLThinker	3B	21.90	20.80	24.72	23.66	20.11	21.76	50.95	64.17	38.81
MMedExpert-R1	2B	23.35	23.02	24.18	28.12	19.54	22.68	53.27	64.64	43.67
LLaVA-Med	7B	19.65	19.43	20.21	22.32	19.54	18.68	30.07	43.68	31.23
HuatuoGPT-V	7B	22.65	21.43	25.81	21.65	20.11	23.76	53.40	75.46	51.27
BiMediX2	7B	22.15	21.23	24.54	22.54	21.24	22.26	42.79	62.42	34.59
Lingshu	7B	26.00	25.44	27.43	28.12	22.09	26.35	54.68	82.85	51.21
MMedExpert-R1	7B	27.50	26.55	29.96	29.91	22.66	28.02	56.78	83.03	52.10

Table 2: Results on the validation set of GMAI-MMBench for clinical VQA tasks. CR denotes Cell Recognition, SAR denotes Surgeon Action Recognition, OR-T denotes Organ Recognition - Thorax, OR-H denotes Organ Recognition - Head and Neck, OR-A denotes Organ Recognition - Abdomen, NT denotes Nervous Tissue, MR denotes Microorganism Recognition.

Base	CR	SAR	OR-T	OR-H	OR-A	NT	MR
MedVLM-R1	41.73	26.08	42.35	41.29	36.32	57.50	36.29
Med-R1	42.60	27.82	40.00	40.00	35.91	65.00	37.03
MedVLThinker	40.86	27.82	38.23	43.87	43.67	52.50	30.37
MMedExpert-R1	42.60	28.69	42.94	50.32	34.28	72.50	39.25
MedGemma	31.30	24.34	51.17	57.41	42.44	55.00	35.55
LLaVA-Med	24.34	13.04	24.11	20.64	31.85	47.50	34.81
HuatuoGPT-V	38.26	22.60	56.47	60.00	49.79	72.50	51.11
BiMediX2	27.49	24.34	33.52	37.41	28.57	35.00	35.55
Lingshu	39.13	27.82	51.17	65.16	50.10	77.50	57.03
MMedExpert-R1	40.00	31.30	60.58	65.16	54.28	80.00	57.77

dominating the 2B/3B tier, while the 7B model leads the "Diagnosis" task with a score of 28.02. This clinical expertise is further corroborated by the granular breakdown in Table 2. MMedExpert-R1 (7B) demonstrates robust capabilities across diverse visual recognition tasks, achieving the highest scores in Cell Recognition (CR) with 40.00 and Microorganism Recognition (MR) with 57.77. Furthermore, it excels in anatomical localization, leading in Organ Recognition - Head and Neck (OR-H) (65.16) and Organ Recognition - Abdomen (OR-A) (54.28). Even the 2B variant displays competitive performance, particularly in Nervous Tissue (NT) recognition (72.50) and Surgeon Action Recognition (SAR) (28.69). These

Table 3: Ablation study of different training strategies and components in MMedExpert-R1. **Unified**: Training on pooled data. **Disentangled**: Training specialized experts. **TIES**: Conflict-aware merging.

Method	DSA		Advantage		CACI		Avg. Score
	Unified	Disentangled	GRPO	GBA	Naive	TIES	
Base	-	-	-	-	-	-	20.90
AM	-	✓(AM)	-	-	-	-	22.30
CAH	-	✓(CAH)	-	-	-	-	22.80
BS	-	✓(BS)	-	-	-	-	19.90
CSI	-	✓(CSI)	-	-	-	-	21.30
Mixed SFT	✓	-	-	-	-	-	22.05
GRPO	-	-	✓	-	-	-	21.35
GBA	-	-	-	✓	-	-	21.90
Mixed SFT + GBA	✓	-	-	✓	✓	-	22.05
DSA + GBA	-	✓	-	✓	✓	-	22.35
Ours	-	✓	-	✓	-	✓	23.35

results indicate that our expert-guided alignment strategy effectively enhances the model's ability to handle complex, domain-specific visual challenges ranging from microscopic identification to surgical context understanding. (More results are shown in the Appendix C.)

5.2.3 Ablation Study

We conduct comprehensive ablation studies to investigate the effectiveness of each component in MMedExpert-R1. The experiments are categorized into three aspects: the impact of Domain-Specific Adaptation, the effectiveness of Reasoning-Specific Adaptation, and the optimization of Conflict-Aware Capability Integration and merging methods. Detailed categories are shown in Table 3.

Impact of Domain-Specific Adaptation. We first evaluate the contribution of the Domain-Specific

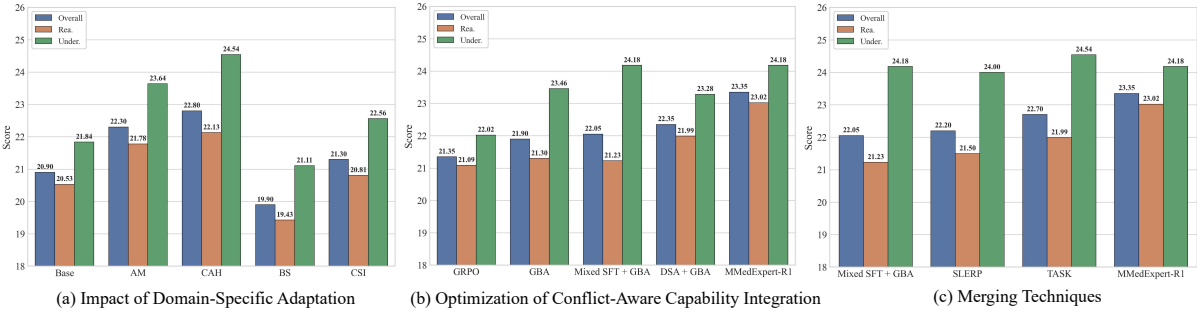


Figure 3: Ablation studies on MMedExpert-R1. (a) illustrates the impact of Domain-Specific Adaptation. (b) shows optimization of Conflict-Aware Capability Integration. (c) demonstrates the superiority of our merging technique.

Adaptation (DSA) stage by training individual experts on different data categories (denoted as AM, CAH, BS, and CSI). As shown in Fig 3 (a), models trained on specific high-quality subsets generally outperform the Base model. Notably, CAH achieves a significant boost, reaching an overall score of 22.80 compared to the Base score of 20.90. It is observed that while some domains like BS may not immediately yield general improvements due to domain shifts, the strong performance of CAH and AM validates our hypothesis: even with a limited amount of data, high-quality, domain-specific instruction tuning can yield substantial performance gains. This justifies our strategy of training distinct experts before aggregation.

Effectiveness of Guideline-Based Advantages. In the second block of Fig 3 (b), we compare the efficacy of standard Group Relative Policy Optimization (GRPO) against our proposed Guideline-Based Advantage (GBA). The results demonstrate that GBA (21.90) consistently outperforms the primitive GRPO (21.35) across all metrics. This improvement suggests that incorporating multi-view perspectives during the alignment phase enables the model to capture more robust feedback gradients, thereby enhancing its reasoning and understanding capabilities more effectively than standard policy optimization methods.

Optimization of Conflict-Aware Capability Integration. We further analyze different strategies for integrating the DSA and GBA. We compare three settings: Mixed SFT + GBA: Mixing all expert data during the DSA stage, followed by GBA training. DSA + GBA: Merging expert models after the DSA stage, followed by GBA training. MMedExpert-R1 (Ours): A multi-stage approach where we perform model merging after both the DSA and GBA stages. As shown in the bottom block of Table 3, the mixed data training (Mixed

SFT + GBA) yields limited improvement (22.05). While merging after DSA (DSA + GBA) improves the score to 22.35, our full multi-stage merging strategy (MMedExpert-R1) achieves the highest performance of 23.35. This indicates that preserving expert specialization through separate training and merging them at multiple stages is superior to simply mixing data or merging only once.

Analysis of Merging Techniques. Finally, we investigate the impact of different model merging algorithms on the final performance. Based on the optimized pipeline, we compare our method against standard merging techniques, including Spherical Linear Interpolation (SLERP) and Task Arithmetic (TASK). As presented in Fig 3 (c), while Task Arithmetic (22.70) outperforms SLERP (22.20) and the mixed baseline, MMedExpert-R1 achieves the best results (23.35). This confirms that our merging strategy effectively retains the distinct capabilities of each expert model without suffering from parameter interference, leading to the most robust aggregated model.

6 Conclusion

In this paper, we presented MMedExpert-R1, a novel MedVLM framework that effectively bridges the gap between limited high-quality data and robust clinical reasoning capabilities. By introducing a pipeline that integrates Domain-Specific Adaptation for expert specialization and Guideline-Based Advantages for precise preference optimization via advantages based on different clinical guidelines, we successfully synthesized a model that excels in complex medical scenarios. Our comprehensive evaluation across four major benchmarks demonstrates that MMedExpert-R1 achieves state-of-the-art performance at both the 2B and 7B parameter scales.

Limitations

Although our framework demonstrates strong performance across standard multimodal medical benchmarks, there are limitations that are practical to address in near-term follow-up work. First, our expert specialization uses four broad LoRA domains (Adult Medicine, Child and Adolescent Health, Brain and Senses, Cancer and Surgical Interventions); introducing finer-grained subdomains (e.g., cardiology, pulmonology, neurology subspecialties) is a straightforward extension that may further improve specialization without architectural changes. Second, although we evaluate on widely used multimodal medical benchmarks, broadening the evaluation suite to include additional datasets and task variants (e.g., more ophthalmology/dermatology sets, longitudinal comparisons, report summarization) using our MedEvalKit would provide more comprehensive validation.

References

Julián N Acosta, Guido J Falcone, Pranav Rajpurkar, and Eric J Topol. 2022. Multimodal biomedical ai. *Nature medicine*, 28(9):1773–1784.

Rawan AlSaad, Alaa Abd-Alrazaq, Sabri Boughorbel, Arfan Ahmed, Max-Antoine Renault, Rafat Damseh, and Javaid Sheikh. 2024. Multimodal large language models in health care: applications, challenges, and future outlook. *Journal of medical Internet research*, 26:e59505.

Haoxuan Che, Haibo Jin, Zhengrui Gu, Yi Lin, Cheng Jin, and Hao Chen. 2025. Llm-driven medical report generation via communication-efficient heterogeneous federated learning. *IEEE Transactions on Medical Imaging*.

Junying Chen, Chi Gui, Ruyi Ouyang, Anningzhe Gao, Shunian Chen, Guiming Hardy Chen, Xidong Wang, Ruifei Zhang, Zhenyang Cai, Ke Ji, and 1 others. 2024. Huatuogpt-vision, towards injecting medical visual knowledge into multimodal llms at scale. *arXiv preprint arXiv:2406.19280*.

Shiqi Chen, Jinghan Zhang, Tongyao Zhu, Wei Liu, Siyang Gao, Miao Xiong, Manling Li, and Junxian He. 2025. Bring reason to vision: Understanding perception and reasoning through model merging. *arXiv preprint arXiv:2505.05464*.

Daya Guo, Dejian Yang, Haowei Zhang, Junxiao Song, Ruoyu Zhang, Runxin Xu, Qihao Zhu, Shirong Ma, Peiyi Wang, Xiao Bi, and 1 others. 2025. Deepseek-r1: Incentivizing reasoning capability in llms via reinforcement learning. *arXiv preprint arXiv:2501.12948*.

Ibrahim Ethem Hamamci, Sezgin Er, Chenyu Wang, Furkan Almas, Ayse Gulnihal Simsek, Sevval Nil Esirgun, Irem Doga, Omer Faruk Durugol, Weicheng Dai, Murong Xu, and 1 others. 2024. Developing generalist foundation models from a multimodal dataset for 3d computed tomography. *arXiv preprint arXiv:2403.17834*.

Sunan He, Yuxiang Nie, Hongmei Wang, Shu Yang, Yihui Wang, Zhiyuan Cai, Zhixuan Chen, Yingxue Xu, Luyang Luo, Huiling Xiang, and 1 others. 2024. Gsco: Towards generalizable ai in medicine via generalist-specialist collaboration. *arXiv preprint arXiv:2404.15127*.

Yutao Hu, Tianbin Li, Quanfeng Lu, Wenqi Shao, Junjun He, Yu Qiao, and Ping Luo. 2024. Omnimed-vqa: A new large-scale comprehensive evaluation benchmark for medical lvm. In *Proceedings of the IEEE/CVF Conference on Computer Vision and Pattern Recognition*, pages 22170–22183.

Xiaoke Huang, Juncheng Wu, Hui Liu, Xianfeng Tang, and Yuyin Zhou. 2025. Medvlthinker: Simple baselines for multimodal medical reasoning. *arXiv preprint arXiv:2508.02669*.

Wisdom Ikezogwo, Saygin Seyfioglu, Fatemeh Ghezloo, Dylan Geva, Fatwir Sheikh Mohammed, Pavan Kumar Anand, Ranjay Krishna, and Linda Shapiro. 2023. Quilt-1m: One million image-text pairs for histopathology. *Advances in neural information processing systems*, 36:37995–38017.

Mingyu Jin, Qinkai Yu, Chong Zhang, Dong Shu, Suiyuan Zhu, Mengnan Du, Yongfeng Zhang, and Yanda Meng. 2024. Health-llm: Personalized retrieval-augmented disease prediction model. *arXiv preprint arXiv:2402.00746*, 10.

Yuxiang Lai, Jike Zhong, Ming Li, Shitian Zhao, and Xiaofeng Yang. 2025. Med-r1: Reinforcement learning for generalizable medical reasoning in vision-language models. *arXiv preprint arXiv:2503.13939*.

Chunyuan Li, Cliff Wong, Sheng Zhang, Naoto Usuyama, Haotian Liu, Jianwei Yang, Tristan Naumann, Hoifung Poon, and Jianfeng Gao. 2023. Llava-med: Training a large language-and-vision assistant for biomedicine in one day. *Advances in Neural Information Processing Systems*, 36:28541–28564.

Tianbin Li, Yanzhou Su, Wei Li, Bin Fu, Zhe Chen, Ziyan Huang, Guoan Wang, Chenglong Ma, Ying Chen, Ming Hu, and 1 others. 2024. Gmai-vl & gmai-vl-5.5 m: A large vision-language model and a comprehensive multimodal dataset towards general medical ai. *arXiv preprint arXiv:2411.14522*.

Tianwei Lin, Wenqiao Zhang, Sijing Li, Yuqian Yuan, Binhe Yu, Haoyuan Li, Wanggui He, Hao Jiang, Mengze Li, Xiaohui Song, and 1 others. 2025. Healthgpt: A medical large vision-language model for unifying comprehension and generation via heterogeneous knowledge adaptation. *arXiv preprint arXiv:2502.09838*.

Jana Lipkova, Richard J Chen, Bowen Chen, Ming Y Lu, Matteo Barbieri, Daniel Shao, Anurag J Vaidya, Chengkuan Chen, Luoting Zhuang, Drew FK Williamson, and 1 others. 2022. Artificial intelligence for multimodal data integration in oncology. *Cancer cell*, 40(10):1095–1110.

Junling Liu, Ziming Wang, Qichen Ye, Dading Chong, Peilin Zhou, and Yining Hua. 2023. Qilin-med-vl: Towards chinese large vision-language model for general healthcare. *arXiv preprint arXiv:2310.17956*.

Ziyu Liu, Zeyi Sun, Yuhang Zang, Xiaoyi Dong, Yuhang Cao, Haodong Duan, Dahua Lin, and Jiaqi Wang. 2025. Visual-rft: Visual reinforcement fine-tuning. *arXiv preprint arXiv:2503.01785*.

Michael Moor, Qian Huang, Shirley Wu, Michihiro Yasunaga, Yash Dalmia, Jure Leskovec, Cyril Zakra, Eduardo Pontes Reis, and Pranav Rajpurkar. 2023. Med-flamingo: a multimodal medical few-shot learner. In *Machine Learning for Health (ML4H)*, pages 353–367. PMLR.

Sahal Shaji Mullappilly, Mohammed Irfan Kurpath, Sara Pieri, Saeed Yahya Alsejari, Shanavas Cholakkal, Khaled Aldahmani, Fahad Khan, Rao Anwer, Salman Khan, Timothy Baldwin, and 1 others. 2024. Bimedix2: Bio-medical expert lilm for diverse medical modalities. *arXiv preprint arXiv:2412.07769*.

Vishwesh Nath, Wenqi Li, Dong Yang, Andriy Myronenko, Mingxin Zheng, Yao Lu, Zhijian Liu, Hongxu Yin, Yee Man Law, Yucheng Tang, and 1 others. 2025. Vila-m3: Enhancing vision-language models with medical expert knowledge. In *Proceedings of the Computer Vision and Pattern Recognition Conference*, pages 14788–14798.

Jiazen Pan, Che Liu, Junde Wu, Fenglin Liu, Jiayuan Zhu, Hongwei Bran Li, Chen Chen, Cheng Ouyang, and Daniel Rueckert. 2025. Medvilm-r1: Incentivizing medical reasoning capability of vision-language models (vlms) via reinforcement learning. In *International Conference on Medical Image Computing and Computer-Assisted Intervention*, pages 337–347. Springer.

Thomas Savage, Ashwin Nayak, Robert Gallo, Ekanath Rangan, and Jonathan H Chen. 2024. Diagnostic reasoning prompts reveal the potential for large language model interpretability in medicine. *NPJ Digital Medicine*, 7(1):20.

Andrew Sellergren, Sahar Kazemzadeh, Tiam Jaroensri, Atilla Kiraly, Madeleine Traverse, Timo Kohlberger, Shawn Xu, Fayaz Jamil, Cian Hughes, Charles Lau, and 1 others. 2025. Medgemma technical report. *arXiv preprint arXiv:2507.05201*.

Yanzhou Su, Tianbin Li, Jiyao Liu, Chenglong Ma, Junzhi Ning, Cheng Tang, Sibo Ju, Jin Ye, Pengcheng Chen, Ming Hu, and 1 others. 2025. Gmai-vl-r1: Harnessing reinforcement learning for multimodal medical reasoning. *arXiv preprint arXiv:2504.01886*.

Dianzhe Tian, Shitao Jiang, Lei Zhang, Xin Lu, and Yiyao Xu. 2023. The role of large language models in medical image processing: a narrative review. *Quantitative Imaging in Medicine and Surgery*, 14(1):1108.

Sheng Wang, Zihao Zhao, Xi Ouyang, Tianming Liu, Qian Wang, and Dinggang Shen. 2024. Interactive computer-aided diagnosis on medical image using large language models. *Communications Engineering*, 3(1):133.

Weiwen Xu, Hou Pong Chan, Long Li, Mahani Aljunied, Ruifeng Yuan, Jianyu Wang, Chenghao Xiao, Guizhen Chen, Chaoqun Liu, Zhaodonghui Li, and 1 others. 2025. Lingshu: A generalist foundation model for unified multimodal medical understanding and reasoning. *arXiv preprint arXiv:2506.07044*.

Dayu Yang, Tianyang Liu, Daoan Zhang, Antoine Simoulin, Xiaoyi Liu, Yuwei Cao, Zhaopu Teng, Xin Qian, Grey Yang, Jiebo Luo, and 1 others. 2025. Code to think, think to code: A survey on code-enhanced reasoning and reasoning-driven code intelligence in llms. *arXiv preprint arXiv:2502.19411*.

Enneng Yang, Li Shen, Guibing Guo, Xingwei Wang, Xiaochun Cao, Jie Zhang, and Dacheng Tao. 2024. Model merging in llms, mllms, and beyond: Methods, theories, applications and opportunities. *arXiv preprint arXiv:2408.07666*.

Jin Ye, Guoan Wang, Yanjun Li, Zhongying Deng, Wei Li, Tianbin Li, Haodong Duan, Ziyan Huang, Yanzhou Su, Benyou Wang, and 1 others. 2024. Gmai-mmbench: A comprehensive multimodal evaluation benchmark towards general medical ai. *Advances in Neural Information Processing Systems*, 37:94327–94427.

Kai Zhang, Rong Zhou, Eashan Adhikarla, Zhiling Yan, Yixin Liu, Jun Yu, Zhengliang Liu, Xun Chen, Brian D Davison, Hui Ren, and 1 others. 2024a. A generalist vision–language foundation model for diverse biomedical tasks. *Nature Medicine*, 30(11):3129–3141.

Xiaoman Zhang, Chaoyi Wu, Ziheng Zhao, Weixiong Lin, Ya Zhang, Yanfeng Wang, and Weidi Xie. 2023. Pmc-vqa: Visual instruction tuning for medical visual question answering. *arXiv preprint arXiv:2305.10415*.

Yiming Zhang, Baoyi He, Shengyu Zhang, Yuhao Fu, Qi Zhou, Zhijie Sang, Zijin Hong, Kejing Yang, Wenjun Wang, Jianbo Yuan, and 1 others. 2024b. Unconstrained model merging for enhanced lilm reasoning. *arXiv preprint arXiv:2410.13699*.

Yuxin Zuo, Shang Qu, Yifei Li, Zhangren Chen, Xuekai Zhu, Ermo Hua, Kaiyan Zhang, Ning Ding, and Bowen Zhou. 2025. Medxpertqa: Benchmarking expert-level medical reasoning and understanding. *arXiv preprint arXiv:2501.18362*.

Appendix for MMedExpert-R1

Abstract.

Appendix A shows the explanation for "four distinct paradigms: (1) differential diagnosis, (2) intuitive reasoning, (3) analytical reasoning, and (4) Bayesian reasoning".

Appendix B details the training hyperparameters.

Appendix C shows the complete results on GMAI-MMBench and OmniMedVQA.

Appendix D shows the visualization results on the MedXpert-MM benchmark.

Appendix E details the cost of computation.

A Four Distinct Paradigms

To clarify how the four paradigms guide distinct reasoning trajectories for the same case, we provide the following definitions and structured examples:

Differential Diagnosis Reasoning. Construct a differential diagnosis list, compare competing etiologies step by step, and eliminate them using imaging and clinical cues.

Example: (1) The lesion is round and circumscribed, favoring benignity. (2) Phyllodes tumor: typically larger, lobulated. (3) Invasive ductal carcinoma with DCIS: irregular, spiculated margins—absent here. (4) Fibroadenoma: smooth, encapsulated mass—matches best.

Intuitive Reasoning. Apply pattern recognition and association of visual features with typical diseases.

Example: (1) Smooth, oval mass with clear borders is intuitively recognized as benign. (2) Absence of calcifications or distortion supports nonmalignant nature. (3) Common benign lesion in this pattern is fibroadenoma.

Analytical Reasoning. Use mechanistic and pathophysiologic deduction based on structural and cellular processes.

Example: (1) Malignancies induce stromal desmoplasia → spiculation (absent). (2) Intraductal lesions form cystic or complex masses (not observed). (3) Metastatic nodules are usually multiple. (4) Benign stromal proliferation forming a smooth, solid encapsulated nodule fits fibroadenoma.

Bayesian Reasoning. Start from prior probabilities, update with new imaging evidence, and infer posterior likelihoods.

Example: (1) Prior: Fibroadenoma most common benign mass in screening-age group. (2) Evidence: Smooth border increases $P(\text{benign})$; absence of distortion decreases $P(\text{malignant})$. (3) Posterior: Highest posterior probability assigned to fibroadenoma after evidence update.

B Implementation Details

Our experiments are conducted using Qwen2-VL-2B-Instruct and Lingshu, the multimodal Large Vision-Language Model (LVLM) equipped with a pretrained visual encoder capable of handling image resolutions up to 401,408 pixels.

For the DSA stage, each domain expert is optimized using Low-Rank Adaptation (LoRA). We apply LoRA to all linear layers with a rank $r = 16$ and scaling factor $\alpha = 32$, utilizing bfloat16 precision. The training process spans 3 epochs with a learning rate of 1×10^{-6} , a batch size of 1, and 8 gradient accumulation steps.

For the Reinforcement Learning (RL) stage, we set group size $G = 8$, clipping parameter $\epsilon = 0.2$, and KL penalty coefficient $\beta = 0.001$. The maximum rollout length is set to 1024. To ensure computational efficiency during distributed training, we utilize DeepSpeed ZeRO-2 optimization.

C Complete Results on GMAI-MMBench

Table 5 shows the complete results on GMAI-MMBench. Meanwhile, we trained MMedExpert-R1 using a subset of 1000 OmniMedVQA dataset, and the results showed a significant improvement, even surpassing the performance of MedVLM-R1 trained with 80% of the data, as shown in Table 4.

Table 4: Comparison of different MLLMs on OmniMedVQA benchmark.

Model	OmniMedVQA
MedVLM-R1	77.38
Med-R1	76.08
MMedExpert-R1	77.93

D Visualization Results

Fig 4 and Fig 5 show the visualization results on the MedXpert-MM benchmark.

E Computational Efficiency Analysis

We provide detailed information on computational cost and latency across all major pipeline compo-

Table 5: Results on the validation set of GMAI-MMBench for clinical VQA tasks.

Base	Total	DD	SG	CR	IQG	SAR	OR-T	BVR	B	OR-H	OR-A	NT	MR	SR	AR	OR-P	M	SWR	C
MedVLM-R1	41.18	48.16	23.01	41.73	32.00	26.08	42.35	44.44	40.00	41.29	36.32	57.50	36.29	30.95	42.96	42.66	32.00	31.42	23.40
Med-R1	40.79	47.45	25.52	42.60	34.00	27.82	40.00	40.74	38.85	40.00	35.91	65.00	37.03	31.84	45.92	30.66	24.00	34.28	23.93
MedVLThinker	38.81	43.16	26.35	40.86	26.00	27.82	38.23	42.96	37.14	43.87	43.67	52.50	30.37	30.95	36.29	20.00	30.00	37.14	32.44
MMedExpert-R1	43.67	52.02	25.94	42.60	34.00	28.69	42.94	42.96	38.28	50.32	34.28	72.50	39.25	31.54	42.96	40.00	26.00	31.42	27.12
MedGemma	45.25	52.73	25.10	31.30	30.00	24.34	51.17	55.55	49.71	57.41	42.44	55.00	35.55	33.63	46.66	41.33	30.00	34.28	22.87
LLaVA-Med	31.23	36.05	23.01	24.34	18.00	13.04	24.11	25.18	22.85	20.64	31.85	47.50	34.81	37.50	37.03	17.33	20.00	24.28	22.34
HuatuoGPT-V	51.27	59.70	29.70	38.26	44.00	22.60	56.47	60.74	49.71	60.00	49.79	72.50	51.11	32.14	49.62	49.33	30.00	38.57	37.76
BiMediX2	34.59	39.34	24.26	29.47	28.00	24.34	33.52	36.29	26.85	37.41	28.57	35.00	35.55	33.63	36.29	37.33	34.00	35.71	19.68
Lingshu	51.21	59.70	26.77	39.13	40.00	27.82	51.17	54.07	52.71	65.16	50.10	77.50	57.03	31.84	45.18	60.66	40.00	28.57	32.44
MMedExpert-R1	52.10	58.71	30.96	40.00	40.00	31.30	60.58	52.59	60.00	65.16	54.28	80.00	57.77	32.44	47.40	70.66	42.00	31.42	30.31

Question: A 39-year-old man presents with a history of an index finger injury sustained 6 months ago that has not improved despite eight weeks of splinting. Radiographs from the time of injury (Figure A) and a recent follow-up (Figure B) are provided. Which of the following statements is accurate regarding open reduction and screw fixation for this type of injury?

Answer Choices: (A) Range of motion of the DIP joint in the affected finger is usually less than 10 degrees post-operatively (B) High risk of symptomatic implant (C) Immobilization of the distal interphalangeal joint is required for 2 weeks post-operatively (D) High rates of post-operative infection are common (E) Open reduction via an approach through the nail bed leads to significant post-operative nail deformity

Correct Answer: (B)

MedVLM-R1 Answer: (E)

MMedExpert-R1 Answer: (B)

Thinking Process:

<think>Answer: B\n\nRationale: Open reduction and screw fixation of a displaced fracture of the proximal phalanx is a stable, salvageable procedure. The DIP joint is usually not immobilized postoperatively (and the nail bed approach can cause nail deformity). Implant loosening is not a common complication of open reduction alone, and postoperative infection rates are low with appropriate wound care and antibiotic prophylaxis. Postoperative ROM of the DIP joint is usually >10 degrees.</think><answer>B</answer>

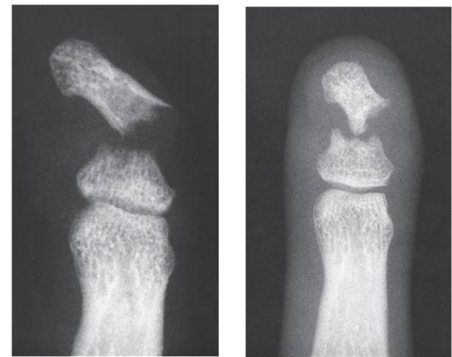


Figure 4: Visualization on MedXpert-MM.

nents to demonstrate deployment feasibility. All estimates are based on experiments conducted on a single NVIDIA A100 GPU.

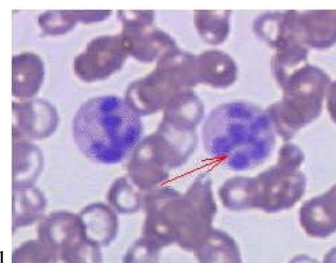
Domain-Specific Adaptation (DSA). Leveraging the lightweight nature of LoRA-based fine-tuning, training on approximately 1,000 samples requires only ≈ 0.4 hours. This low overhead facilitates rapid adaptation to new domains.

Guideline-Based Advantages (GBA). RL fine-tuning is the most compute-intensive stage, requiring ≈ 13 hours for 1,000 samples. The increased computational cost is primarily driven by the need for multi-sample generation per iteration and the calculation of KL-divergence for policy regularization.

Conflict-Aware Capability Integration. The merging of domain experts is highly efficient, taking ≈ 5 minutes per merge operation. Crucially, this process results in a single consolidated model, incurring **negligible additional latency** during inference compared to a standard base model.

Question: "A 60-year-old female presents to a geriatrics clinic reporting fatigue and memory issues for the past two months. She maintains a positive mood without sleep disturbances or loss of interest. The patient follows a vegetarian diet, lives independently, and has local siblings for support. She is not currently taking any medications. Physical examination reveals lemon-tinted skin and tongue papillae loss. Neurological assessment shows impaired vibratory sensation and proprioception. Laboratory findings indicate:
Hemoglobin 10.5 g/dL
Hematocrit 31.3%
Mean corpuscular hemoglobin concentration 28% Hb/cell
Mean corpuscular volume 115 μm^3
Leukocyte count 4500/mm³
Platelet count 100,000/mm³
Given the peripheral blood smear findings, what is the most likely pathophysiologic mechanism responsible for this patient's anemia?"

Answer Choices: (A) Disturbance in the conversion of methylmalonyl CoA to succinyl CoA (B) Decreased supply of dihydrofolate reductase (C) Inhibition of dihydrofolate reductase (D) Deficiency of orotidylate decarboxylase (E) Methyltetrahydrofolate trap",



Correct Answer: (E)

MedVLM-R1 Answer: (C)

MMedExpert-R1 Answer: (E)

Thinking Process:

"<think>Answer: E. Methyltetrahydrofolate trap.
<input type="radio" value="E"/> Rationale: The peripheral smear shows macrocytic anemia with a low MCV (115 μm^3) and a high MCHC (28%) — classic for a methyltetrahydrofolate trap. A methyltetrahydrofolate trap occurs when folate is converted to tetrahydrofolate (and then to H4) by dihydrofolate reductase (DHFR) but is then trapped by methylmalonyl-CoA in the tricarboxylic cycle, preventing conversion of methylmalonyl-CoA to succinyl-CoA. This trapping prevents folate conversion and causes macrocytic anemia.</think><answer>E</answer>"

Figure 5: Visualization on MedXpert-MM.